On the Atmospheric Response to Oyashio Extension Front Disturbance and Mesoscale SST Variations

CLAUDE FRANKIGNOUL,[a,b] RICHARD HALL,[c,d] YOUNG-OH KWON,[b] AND ARNAUD CZAJA[c]

[a] *Sorbonne University, LOCEAN/IPSL, Paris, France*
[b] *Woods Hole Oceanographic Institution, Woods Hole, Massachusetts*
[c] *Imperial College London, London, United Kingdom*
[d] *University of Sheffield, Sheffield, United Kingdom*

(Manuscript received 11 February 2025, in final form 19 May 2025, accepted 10 July 2025)

ABSTRACT: Using a regional atmospheric model at 27-km resolution over the western North Pacific, we explore the sensitivity of the atmospheric response to sea surface temperature (SST) anomalies associated with meridional shifts of the Oyashio Extension (OE) front. Twenty different SST conditions are prescribed by adding SST anomalies in different years of 1979–2016 to a base SST state taken on a February 2013 day with a relatively neutral SST distribution. The model is integrated for a single storm duration and the entire February 2013, using identical initial and lateral boundary conditions. The differences between the responses to the 10 highest and lowest SST anomalies are highly significant and baroclinic. Simulations with the extreme positive and negative SST anomalies and their decomposition into spatial mean and residuals indicate that the large-scale and storm-track responses are determined by the spatial mean SST anomalies and are insensitive to the residual mesoscale SSTs. This holds at 10-km atmospheric resolution, where the responses remain similar and are dominated by the impact of the spatial mean SST anomalies, except for slight differences in the storm-track response and stronger vertical motions. We also investigate the influence of the central region (155°–164°E) of the OE that often has parallel or indistinct frontal zones in part linked to mesoscale eddy activity, as described by a frontal disturbance index (FDI). Differences between the response to the 10 highest and lowest FDI cases are small and lack statistical significance. Mesoscale SST variations thus had very little impact on the large-scale atmospheric response.

SIGNIFICANCE STATEMENT: Several modeling studies have suggested that mesoscale eddy variability in western boundary current regions has a strong influence on the storm track and the atmospheric circulation. However, these studies were generally based on simulations using spatially smoothed SSTs so that the mean SST gradients are weakened. Using a regional model without such spatial smoothing, we show that the atmospheric response to SST anomalies in the Oyashio Extension region is determined by their spatial mean and is largely insensitive to residual mesoscale SST variations. These results have to be mitigated against the smallness of the spatial domain simulated and the fact that we are only considering one single February month.

KEYWORDS: Atmosphere-ocean interaction; Fronts; Storm tracks; Winter/cool season; Regional models

1. Introduction

Many studies have shown that mesoscale sea surface temperature (SST) variations affect the marine atmospheric boundary layer and surface wind (Chelton et al. 2004; Xie 2004 among many others, as reviewed, e.g., by Small et al. 2008; Seo et al. 2023). This local response would drive nonlocal responses in the storm track and large-scale atmospheric processes and explain, in particular, how ocean fronts associated with the midlatitude western boundary currents (WBCs) and their extensions influence the atmospheric circulation (see reviews by Kelly et al. 2010; Kwon et al. 2010; Czaja et al. 2019). Observational studies have detected the influence of WBC front variability onto the atmosphere in the North Pacific and the North Atlantic, using either frontal displacement (Joyce et al. 2009, 2019; Frankignoul et al. 2011; O'Reilly and Czaja 2015; Révelard et al. 2016; Famoos Paolini et al. 2022) or SST variability in a region centered on the oceanic front (Taguchi et al. 2012; Wills et al. 2016; Wills and Thompson 2018) as a marker of frontal variability. The two were deemed equivalent since SST variability is enhanced along the fronts and northward frontal shifts are accompanied by warm SST anomalies, and vice versa for a southward shift. However, it does not inform whether it is the displacement of the sharp mesoscale fronts that largely affects low-level baroclinicity or the change in SST and diabatic heating that mostly control the atmospheric response (cf. Booth et al. 2012). Observational studies of individual cyclone development along SST fronts suggest that the change in SST dominates since, for example, Tsopouridis et al. (2021) found no direct effect of the SST front on cyclone intensification in the Kuroshio region. The prevalence of the surface latent heat flux associated with the absolute SST was confirmed by the idealized channel simulations of Bui and Spengler (2021; see also Haualand and Spengler 2020).

Sensitivity studies with atmospheric general circulation models (AGCMs) have also been used to investigate how fronts force the atmospheric circulation. A standard method is to compare simulations using observed or climatological

Corresponding author: Claude Frankignoul, claude.frankignoul@locean.ipsl.fr

DOI: 10.1175/JCLI-D-25-0083.1

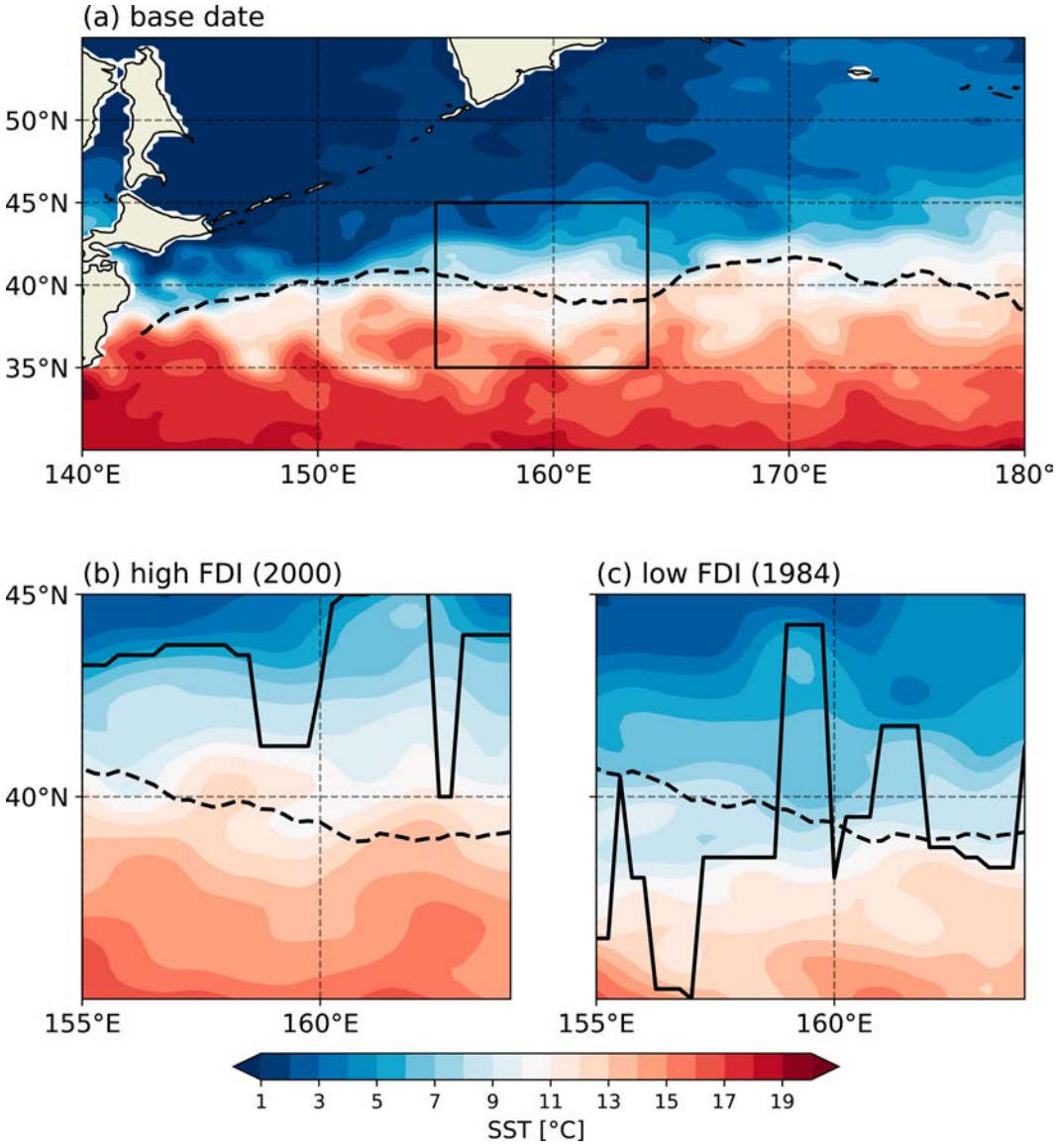

FIG. 1. (a) SST (°C) of the base state in the whole 32°–55°N, 140°E–180° WRF domain and in the domain of definition of the (b) highest and (c) lowest mean SST difference. The dashed line shows the climatological position of the maximum SST gradient during February, and the continuous line indicates the latitude of the maximum SST gradient in the two FDI domains. The box in (a) indicates the domain where the SST anomalies are applied, equivalent to the domains in (b) and (c).

SSTs with simulations using spatially smoothed SSTs so that the mean SST gradients are weakened, which leads to large alongfront dipolar SST anomalies (e.g., Small et al. 2014; Piazza et al. 2016; Parfitt et al. 2016; Kuwano-Yoshida and Minobe 2017). The same method has been used to investigate the impact of oceanic mesoscale eddies on the atmospheric circulation (Ma et al. 2015, 2017; Liu et al. 2021), showing substantial impacts of the eddy variability on storm track and jet stream. However, spatial smoothing alters the absolute SST, so that specific impacts of the mesoscale variations are difficult to single out. Chakravorty et al. (2024) did use ensemble mean ocean simulations rather than spatial smoothing to investigate the impact of Gulf Stream mesoscale variability on traveling weather systems and found a clear impact on the marine boundary layer and weaker signals in the free troposphere. Foussard et al. (2019) investigated eddy influence by adding mesoscale eddies near a front without altering the zonal-mean SST and its gradient and found robust local asymmetric eddy impacts and a poleward shift of mean upper zonal wind and eddy variance. However, the simulations were made in highly idealized conditions (periodic channel with a zonally symmetric front), and further investigations are needed.

Here, we use a different approach in the context of the Oyashio Extension (OE) influence on wintertime atmospheric

TABLE 1. Dates used to calculate the FDI value and the mean SST difference (K, after tapering) for that date from the SST base date (16 Feb 2013), calculated over 150°–170°E, 35°–45°N. The highest and lowest FDI and SST differences are highlighted (bold).

High FDI date	High FDI value	High FDI mean SST diff	Low FDI date	Low FDI value	Low FDI mean SST diff
9 Feb 2000	**1.12**	**0.70**	11 Feb 1996	−0.56	−0.23
20 Feb 2012	0.75	−0.19	3 Feb 2007	−0.51	0.15
15 Feb 2001	0.69	−0.14	29 Feb 2016	−0.5	−0.04
9 Feb 2003	0.61	0.1	11 Feb 1995	−0.49	−0.14
3 Feb 2013	0.58	0.14	15 Feb 2011	−0.48	0.6
1 Feb 2005	0.56	0.37	22 Feb 2014	−0.47	0.28
21 Feb 2002	0.49	0.03	**29 Feb 1984**	**−0.45**	**−0.75**
17 Feb 1997	0.47	−0.14	14 Feb 1998	−0.42	−0.25
11 Feb 1990	0.45	0.26	25 Feb 1986	−0.4	−0.53
7 Feb 2010	0.43	0.39	3 Feb 2006	−0.39	−0.2
Mean	0.62	0.15		−0.47	−0.11

circulation by investigating the impact of SST anomalies associated with OE variability in realistic conditions without smoothing the base SST field. This is done using short simulations with a regional ocean model at 27-km and, in some cases, 10-km resolution, which may suffice to simulate SST impact on cyclone development (e.g., Willison et al. 2013). A novelty of our approach is that simulations are made to differentiate between the influence of the SST anomalies, their spatial mean, and the residuals. We find that it is the spatial mean of the SST anomaly differences that controls the atmospheric response, while mesoscale SST variations have very little impact.

2. Method

The Weather Research and Forecasting (WRF) Model, version 4.5 (Skamarock et al. 2008; Powers et al. 2017), with 45 vertical levels is used in the ~32°–55°N, 140°E–180° domain, which includes the Kuroshio–OE (KOE) and covers the region of the western Pacific across which most storms track (i.e., approximately the domain in Fig. 1a). The parameterizations include the Purdue Lin microphysics scheme (Chen and Sun 2002), the new Tiedtke cumulus physics parameterization (Zhang and Wang 2017), Rapid Radiative Transfer Model for general circulation models (RRTMGs) radiation schemes (Iacono et al. 2008), YSU planetary boundary layer (Hong et al. 2006), revised MM5 surface layer (Jimenez et al. 2012), and unified Noah land surface model (Tewari et al. 2004). The model is used at 27- and 10-km resolution. We use daily SST data from the National Oceanic and Atmospheric Administration (NOAA) optimum-interpolation (OI), version 2.1, AVHRR-only dataset (Reynolds et al. 2007) in the 1979–2016 period with 0.25° resolution, which is suggested to be superior to ERA5 SST data (Hersbach et al. 2020) when resolving mesoscale activity in the KOE region (Hall et al. 2025; Sroka et al. 2022).

Part of our initial motivation was to explore the role of the central region (155°–164°E) of the OE, where the SST front tends to be diffuse, and parallel or indistinct frontal zones in part linked to mesoscale eddy activity are often found (Fig. 1a). The frontal disturbance index (FDI) was introduced by Hall et al. (2025) to quantify the extent to which the location of the OE front departs from the climatology. At a given time, the FDI is defined as the root-mean-square (rms) deviation of the anomalies of the latitude of maximum SST gradient (previously standardized) over the 155°–164°E longitudes. It is thus proportional to the mean absolute magnitude of the displacement from climatology in the domain. A higher FDI indicates a higher overall departure from the climatological mean, as illustrated in Fig. 1b for a high FDI (the SST front remains north of the climatological front), and a lower FDI indicates smaller departures as in Fig. 1c (the SST front is scattered around its climatological position, leading to a lower rms). Here, we use daily FDIs, resulting in more noisy fields than those in Hall et al. (2025). The climatological mean FDI is then removed to create positive and negative FDI values.

The analysis focuses on February 2013, a month with a typical range of storms and a relatively neutral FDI. We find the 10 lowest and highest February FDI dates from the 1979–2016 period and use these to prescribe the SST field within the 150°–170°E, 35°–45°N box, while the SST elsewhere is that of 16 February 2013 (the SST base state, Fig. 1a). Each of the

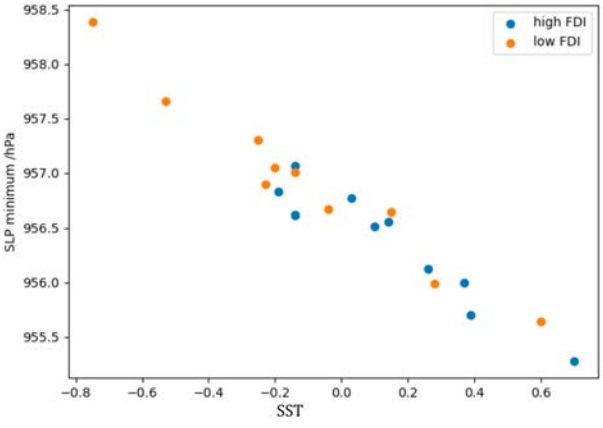

FIG. 2. Scatterplot of the minimum SLP (hPa) on the mean SST (°C) for the 20 FDI cases at 27-km resolution.

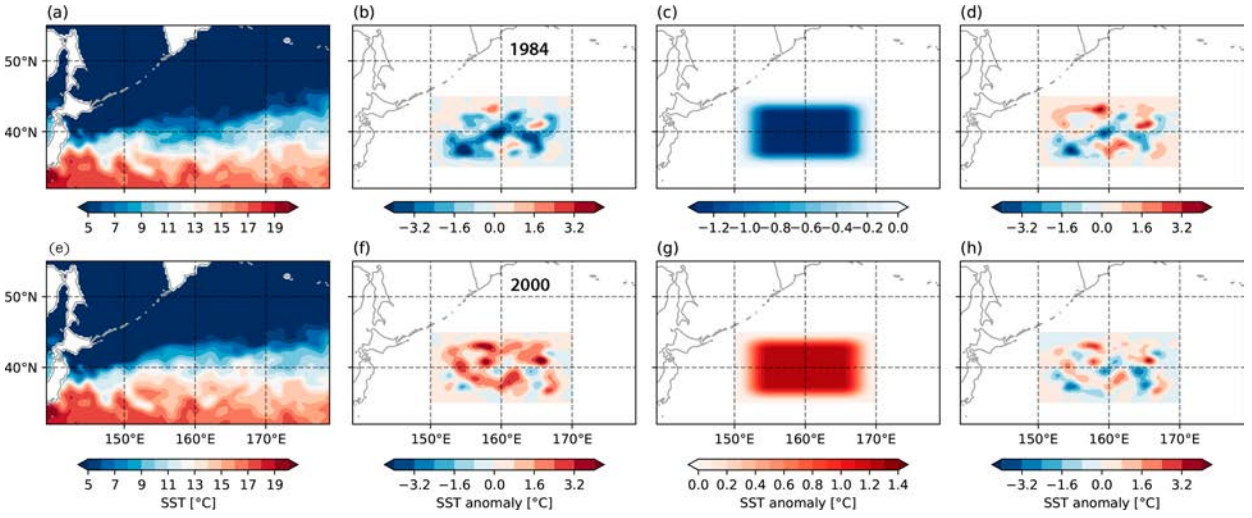

FIG. 3. SST field associated with the (a) lowest and (e) highest SST, (b),(f) corresponding SST anomalies and (c),(g) their decomposition into constant spatial mean and (d),(h) residual SST (°C) after tapering. Note the changes of scale.

10 highest (lowest) dates is taken from a different year, to ensure independence (Table 1). For each model run, the difference between the SST field for the date of the high or low FDI value and the SST base date is added to the base state over 150°–170°E, 35°–45°N. These difference fields have a cosine taper (with tapered section half the whole signal length) applied along both longitude and latitude to ensure a smooth transition with the base state outside the box. Importantly, high FDIs tend to correspond to large positive SST anomalies averaged over the box and low FDIs to negative ones (0.4 correlation).

The model is run for 1 month, using for each run the same initial conditions and the same weather system setup (3-hourly lateral boundary conditions taken from ERA reanalysis in February 2023 at 0.25° horizontal resolution). The SST remains constant; hence, differences between runs are only affected by the prescribed SST anomalies. Note that no smoothing is applied to the base state, contrasting with studies (e.g., Ma et al. 2015, 2017) where spatial SST smoothing filters mesoscale eddies but also weakens the mean SST front so that the effect of the former is not distinguished from the latter. The temporal resolution of the model output is 3 hourly. We also examine the evolution of sea level pressure (SLP) minimum for an individual storm (15–20 February 2013) using a 1-h output resolution.

Additional experiments are run by replacing the SST anomalies added to the base state in 150°–170°E, 35°–45°N by either their spatial mean or the residual mesoscale features.

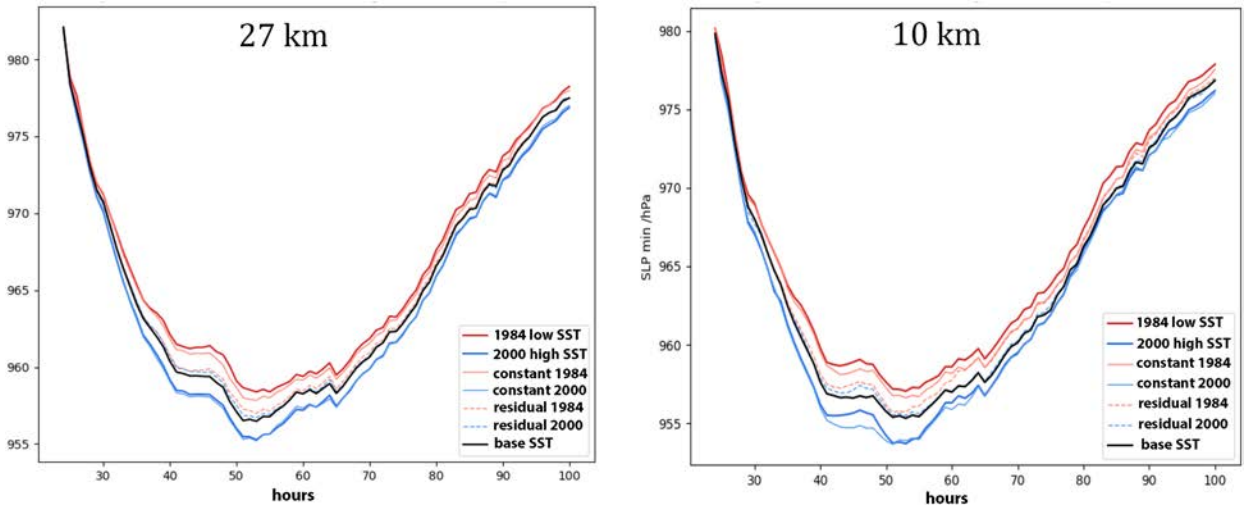

FIG. 4. SLP evolution for the lowest (red) and highest (blue) mean SST states for the single storm of 15–20 Feb 2013 decomposed into response to mean and residual SST, as indicated in the legend using the (left) 27-km and (right) 10-km model resolution. The SLP evolution for the base SST state is shown in black.

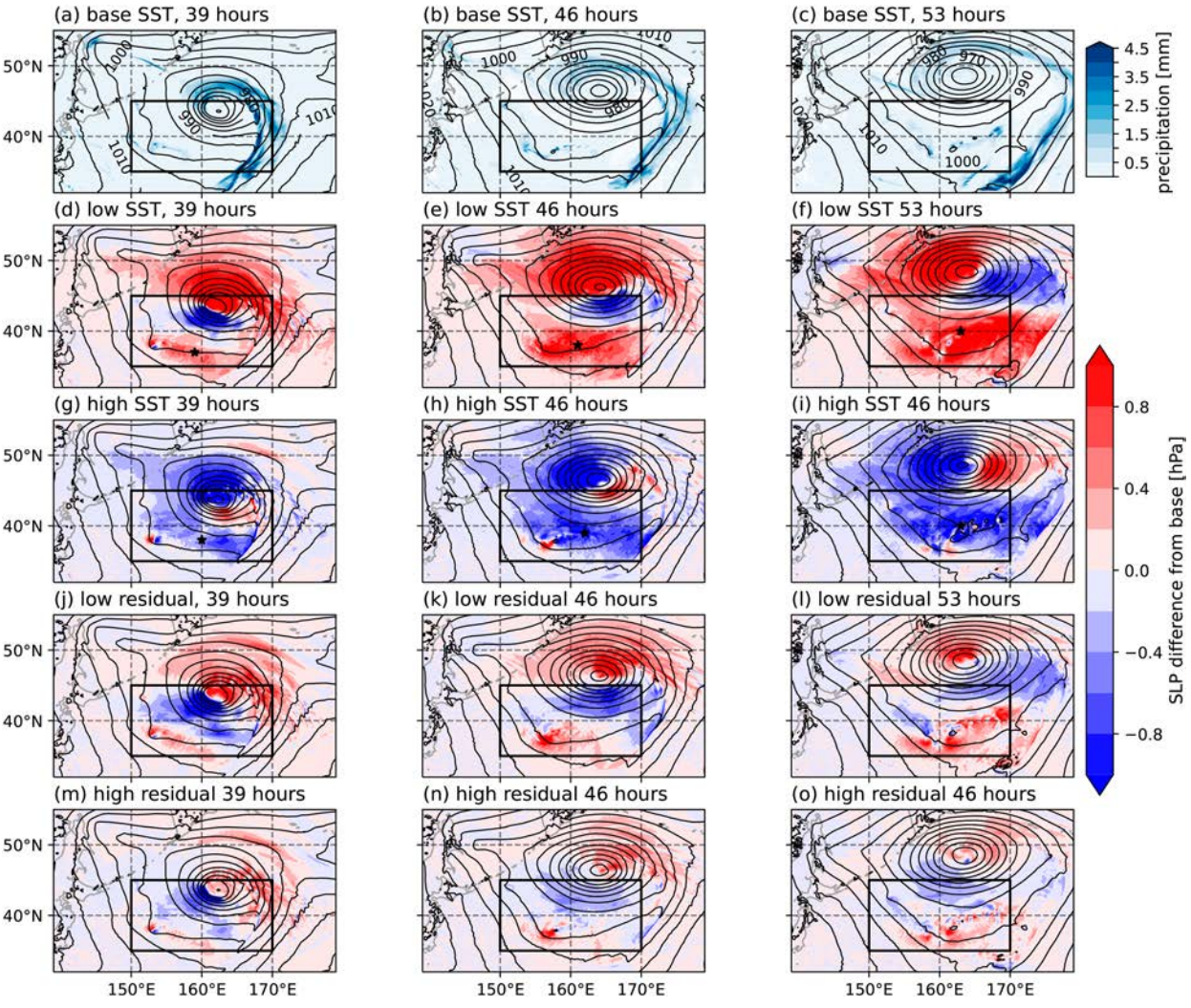

FIG. 5. (top) Evolution (from left to right) of SLP (contours) and precipitation (shading) for the base SST state as the storm passes by; the simulation times are indicated. SLP difference (shading) from the base response for (second row) low SST, (third row) high SST, and SST residual in the (fourth row) low and (bottom) high cases. The contours indicate SLP, and the star in (d)–(i) points to the shallow SLP response.

3. Results

a. A single storm case

The SLP evolution for simulations with the SST anomalies from the 10 highest and lowest FDI cases, and in particular its minimum during the storm of 15–20 February 2013, shows at 27-km resolution practically no difference between the positive and negative FDI cases (not shown). However, the minimum SLP shows a clear linear dependence on the spatial mean SST anomaly associated with each FDI, with higher SST leading to lower SLP (Fig. 2). The SLP deepening is small but highly significant, about -2.1 hPa °C^{-1}.

To investigate how the SST influences the SLP, the SST anomalies of the extreme positive and negative mean SST differences (bold in Table 1) were decomposed into their constant spatial mean and residuals with zero spatial mean, as shown after tapering in Fig. 3. The storm was simulated by adding the SST anomalies or their decomposition to the SST base state. In both cases, the SLP evolution and its minimum using the mean SST closely resemble those for the full SST, while the SST residuals have little influence limited to a very slight increase in the minimum SLP (Fig. 4, left). Using the WRF Model at 10-km resolution instead of 27 km showed similar evolutions, although the response to the SST residuals is larger, in particular, for low SST, where the minimum SLP increase becomes similar to that of the mean SST when the storm passes by (Fig. 4, right). However, the changes in the minimum SLP do not fully represent the SST impacts, as illustrated by three snapshots at 10-km resolution (Fig. 5). As the center of the storm (the SLP minimum) passes above the SST anomaly and moves northward, the SLP response to the full SST anomaly evolves nearly symmetrically (second and third

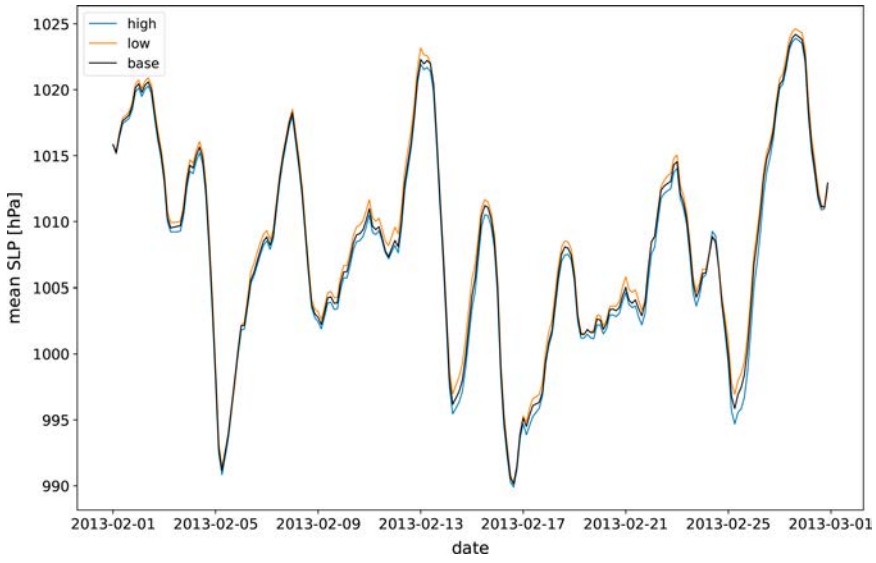

FIG. 6. Minimum SLP evolution over the FDI domain (155°–164°E) at 27-km resolution for the base SST (black), and the highest SST (red) or lowest SST anomaly (blue) simulations in February 2013.

rows in Fig. 5), with a shallow pressure anomaly (high pressure for negative SST anomaly, low pressure for positive one, as marked by a star) in the southern part of the cold sector. This is capped by descending cold air. The anomalous SLP dipoles seen further north extend throughout the troposphere and reflect small shifts in the storm track caused by the prescribed SST anomalies. They essentially disappear if the center of the storm is adjusted such that they are aligned with that of the base SST state, while the shallow SLP anomaly further south remains (not shown). The response to the residual SST (bottom two rows in Fig. 5) has shorter scale and smaller magnitude. It is rather similar in the low and high cases, albeit stronger in the low case. The contribution of the response to the residual SST to the minimum SLP (Fig. 4) is sensitive to its detailed pattern, but its overall impact remains small. In summary, the storm is primarily sensitive to the SST anomaly magnitude, not to its mesoscale variations.

b. *Monthly simulations for the two extreme mean SST differences*

To further investigate the role of mesoscale SST fluctuations in the two extreme SST anomaly cases, the monthly mean responses to the highest and lowest mean SST differences and their decomposition (Fig. 3) were compared at 27- and 10-km resolution. As illustrated in Fig. 6, there are only very small minimum SLP differences with the base run, suggesting that the SLP variability is strongly constrained by the lateral boundary conditions, presumably reflecting the smallness of the WRF domain. Nonetheless, systematic minimum SLP anomalies on the order of 1 hPa are seen throughout the runs with lower SLP for positive SST anomalies and higher SLP for negative SST anomalies, suggesting that monthly averages should be indicative of the SST influence.

At 27-km resolution, the monthly response difference between the high and low mean SST differences is baroclinic, with an SLP low slightly downstream of the positive SST anomaly (Fig. 7a) and an upper-tropospheric high shifted northeastward, as shown by the geopotential height at 300 hPa (Z300; Fig. 7d). The storm-track response, as represented by the standard deviation of Z300, is a dipole that leads to a northward shift of the storm track (Fig. 7g). The response differences are small and essentially due to the spatial mean SSTs (Figs. 7b,e,h), with negligible SST residual impacts (note the changes of scale for the latter, Figs. 7c,f,i).

The SLP and Z300 responses are similar at 10-km resolution (Fig. 8), although they extend a little northward, but the bipolar storm-track response changes to a slightly stronger and narrower tripolar one (Fig. 8g). Although the response differences remain determined by the mean of the SST anomalies, the response to the SST residuals is larger than at 27-km resolution, in particular for the storm track where it opposes the response to the mean SST, with about half its amplitude (Fig. 8i).

As shown by zonal (Figs. 9a,c) and meridional (Figs. 9b,d) averages of the mean vertical velocity differences over the SST box, there are ascending motions above warmer SSTs with descending motions near the zonal and meridional edges of the SST anomaly, with little dependence on resolution but for finer structure at 10-km resolution. There is little detectable influence on the zonal and meridional means of the response to the residual SSTs at 27-km resolution, but a small response at 10-km resolution (not shown). Correspondingly, the total precipitation difference averaged over the SST anomaly box changes little and is even slightly smaller at 10 km than at 27-km resolution, with negligible mesoscale impact. However, individual convective cells are more intense and reach slightly higher at 10-km resolution. This is shown by meridional averages over the SST box of the standard deviation differences of

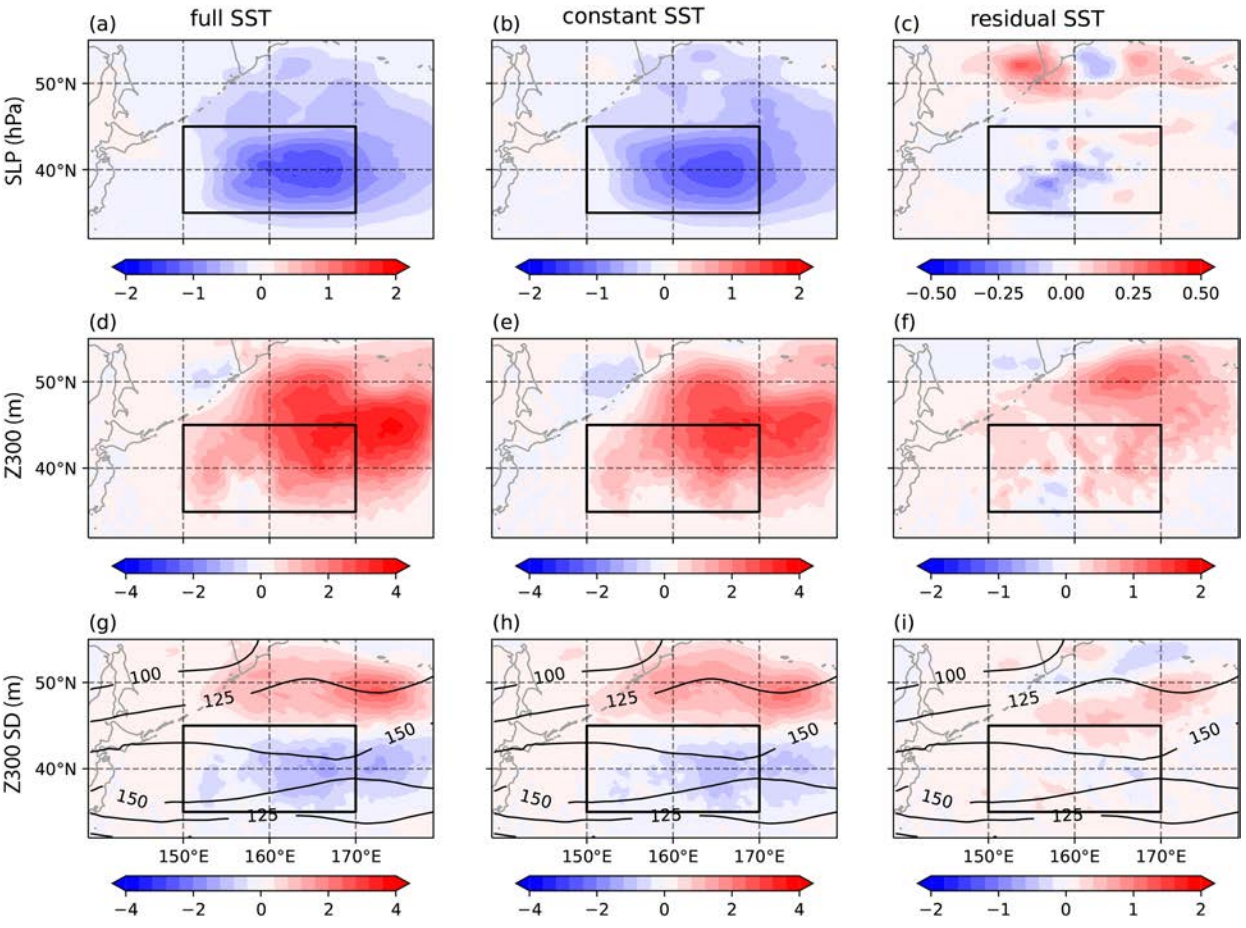

FIG. 7. February 2013 mean difference between the response to the highest and lowest mean SST difference for (from top to bottom) SLP (hPa), Z300 (m), and standard deviation of Z300 (m) at 27-km resolution for (a),(d),(g) full, (b),(e),(h) constant, and (c),(f),(i) residual SST. The box denotes the location of the SST anomalies. Contours in (g), (h), and (i) denote the averaged standard deviation of Z300 (m).

vertical velocity between the responses to the high and low spatially averaged SST (Fig. 10, left panels) and the corresponding SST residuals (Fig. 10, right panels) at 27-km (top) and 10-km (bottom) resolution. Interestingly, the spatial variability of vertical velocity is primarily determined by the model resolution, not by the mesoscale features of the SST anomalies, so that the response differences for full SSTs are very similar to those for the spatially averaged SSTs (not shown). In summary, there are stronger, narrower ascending and descending motions at 10-km resolution, but their averages over the SST box are similar to those at 27-km resolution, consistent with the lack of substantial resolution dependence of the large-scale responses.

In summary, the resolution difference between 27 and 10 km has little impact on the baroclinic large-scale response to the SST anomalies, but higher resolution leads to stronger vertical motions and a somewhat different, albeit not stronger, storm-track response, although local precipitation is barely affected. However, the response dependence on resolution may be hindered by the limited $1/4^\circ$ SST resolution, and SST anomalies with much higher resolution should be used for more robust investigations. In any case, 27-km resolution suffices to further investigate SST influence in the present setup.

c. *February 2013 response to 10 high and 10 low SST/FDI at 27-km resolution*

None of the mean response differences for various atmospheric variables between 10 high and 10 low FDIs are significant based on the false discovery rate (FDR; Wilks 2016) test, but their patterns (not shown) are highly similar to the stronger, significant response differences between the 10 warmest and coldest SST anomalies (Fig. 11). As the correlation between FDI and SST in Table 1 is 0.4, it is likely that the weaker responses to FDI largely reflect the responses to the corresponding spatial mean SST. This was confirmed by composite differences based on a subset of 15 cases with uncorrelated FDI and SST (omitting the 1st, 6th, 9th, 17th, and 18th cases in Table 1) (not shown). We thus only focus on the mean response differences between the 10 largest and the 10 smallest SST anomalies, which are FDR significant.

The mean composited SST differences are displayed in Fig. 12 (top). The mean response differences for SLP, Z300,

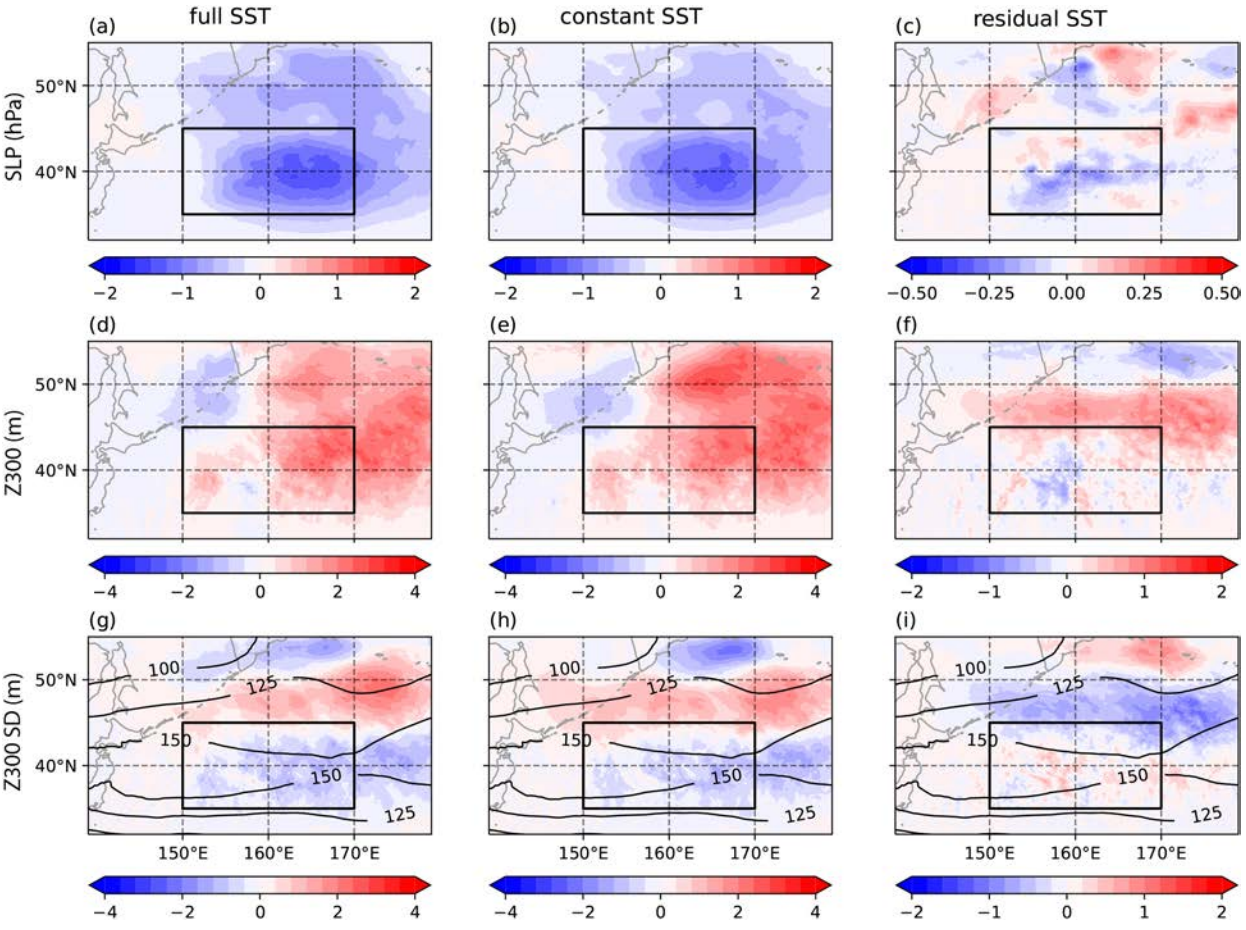

FIG. 8. As in Fig. 7, but for 10-km resolution.

and storm track are highly significant and baroclinic (Fig. 11), broadly resembling the response differences between the two extreme mean SST difference cases (cf. with Fig. 7), but with correspondingly smaller amplitudes. The responses are small but robust, as their patterns remain very similar when limiting the composited differences to the uncorrelated FDI/SST subset (not shown). The mean vertical velocity response largely shows ascending motions above positive SST differences, even reflecting mesoscale SST variations, while descending motions mostly occur north of the SST anomalies, perhaps because of the northward shift of the storm track (Fig. 11, bottom). However, FDR significance is limited. Note that the downward motion along the southern edge of the domain is likely a mass conservation artifact of the nesting of the WRF Model.

Unfortunately, a lack of resources prevented us from performing these simulations at 10-km resolution, but broadly similar results are expected in view of section 3b.

4. Conclusions

The influence of the extent to which the OE SST front departs from climatology on the North Pacific atmosphere in late winter was investigated with a regional atmospheric model. This was done by adding SST anomalies at 0.25° resolution corresponding to 10 high and 10 low daily FDIs to a base-state SST taken from a February day with neutral FDI, using identical initial and lateral boundary conditions in all runs. Simulations of a 5-day storm and the monthly mean for February 2013 showed negligible dependence on the FDI, while the response differences between high and low SST anomalies were highly significant, suggesting a broadly linear dependence on SST. The responses are baroclinic with an SLP low downstream of positive SST and a northward shift of the storm track. However, they have small amplitude, presumably because they are strongly constrained by the lateral boundary conditions of the small domain considered. Additional simulations showed that the atmospheric response is primarily driven by the spatial mean of the SST anomalies and not by the mesoscale SST residuals.

Although going from 27- to 10-km resolution did not affect the large-scale SLP and Z300 response differences between the two extreme mean SST difference cases, the higher resolution led to slightly different impacts on the storm track and stronger vertical motions, albeit without influence on precipitation averaged over the SST box. The

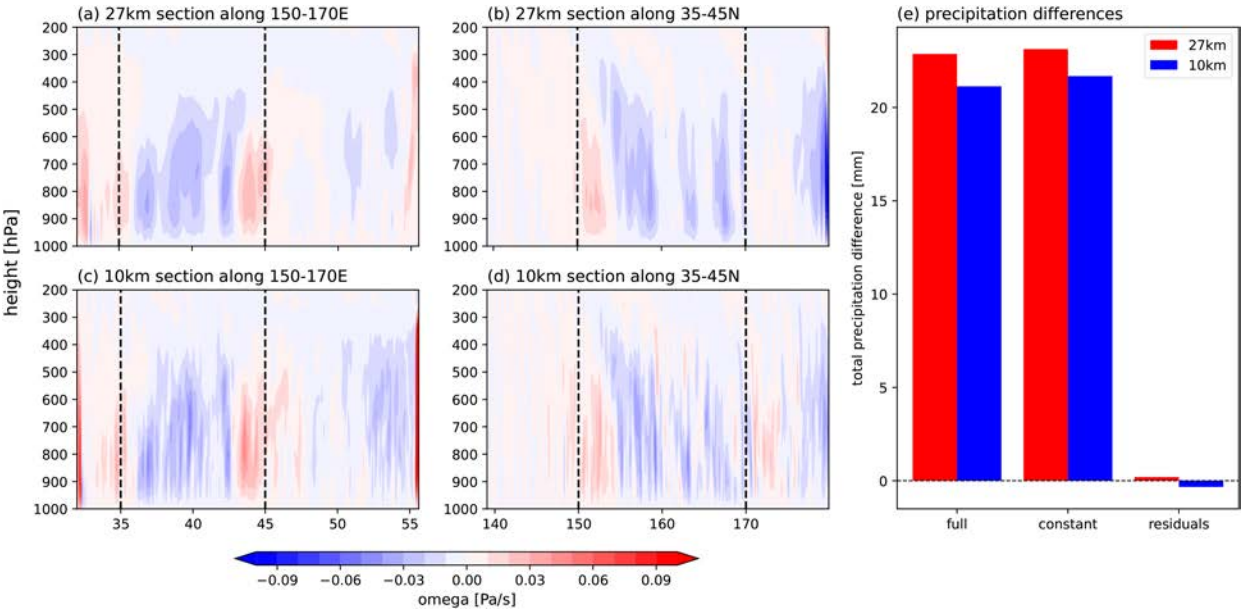

FIG. 9. (left two) Monthly mean vertical velocity difference (Pa s^{-1}) between the response to the highest and lowest mean SST difference at (top) 27-km and (bottom) 10-km resolution for (left) zonal and (right) meridional averages over the prescribed SST anomaly. The dashed vertical lines indicate the corresponding extent of the prescribed SST anomaly. (right) Monthly mean precipitation differences averaged over the SST box at 27-km (red) and 10-km (blue) resolution, for full, constant, and residual SST, as indicated.

specific influence of the mesoscale SST residuals was negligible at 27-km resolution but discernable at 10-km resolution for storm-track activity and vertical velocity, but without significant impact on SLP, Z300, and averaged precipitation.

Larson et al. (2024) found much more intense responses to SST variability in a control simulation of a climate model when increasing its resolution from 1° to 0.25°, stressing the need for high spatial resolution. The limited dependence on resolution found in this study when going from 27- to 10-km resolution suggests that the benefits of going to higher resolution than 0.25° might be limited, but it is in contradiction with the simulations of Schemm (2023), who found enhanced poleward cyclone propagation and more rapid amplification when going from 20- to 5-km resolution, albeit limited to the highest cyclone strength percentiles and occurring during their early and most intense growth phase. However, they were highly idealized simulations (aquaplanet in end of March conditions) covering a very large range of cyclone strength as 10 perpetual years were simulated, while our small set of WRF simulations are constrained by boundary conditions from a single February month that may not be representative of extreme cyclone activity. Clearly, realistic simulations in a larger domain and in more diverse conditions would be needed to further assess the impact of higher resolution on simulated extratropical cyclones.

That the model response is essentially controlled by spatially uniform (before tapering) SST, and largely insensitive to its mesoscale features is seemingly inconsistent with the studies of Ma et al. (2015, 2017) and Liu et al. (2021), who found large impacts of oceanic mesoscale fronts and eddies in the Kuroshio Extension region on storm track, precipitation, and large-scale atmospheric circulation. The difference with our results may largely occur because there is no smoothing of the SST base state in our simulations, unlike in these studies, where spatial SST smoothing also reduced the large-scale SST front so that mesoscale eddy impact was not distinguished from that of changes in the base SST state. On the other hand, our results seem consistent with the coupled model simulations of Small et al. (2019), who found with different ocean resolutions that changes in absolute SST between experiments had a much larger effect than differences in SST gradient, and with the atmospheric simulations of Wills et al. (2024) who found that the response was more sensitive to the warm part of (idealized) SST anomalies than to the meridional SST gradient. They are also in agreement with studies of individual cyclone development along SST fronts that found that cyclone intensification was mainly influenced by absolute SST, with no direct effect of SST fronts (e.g., Tsopouridis et al. 2021; Bui and Spengler 2021).

Our simulations suggest that SST anomalies along the OE front and probably other WBCs may provide a more robust picture of the influence of WBC variability on the large-scale atmospheric circulation than indices of large-scale frontal displacements, as used in Frankignoul et al. (2011) and many others (see section 1), or indices linked to the scatter of front location by mesoscale eddy activity independently on frontal strength, as the FDI in Hall et al. (2025). This may explain the higher statistical significance of response studies that use SST anomalies averaged over the mean WBC location as the WBC variability index (e.g., Wills and Thompson 2018). Note that in this study, the correlation between the mean SST and

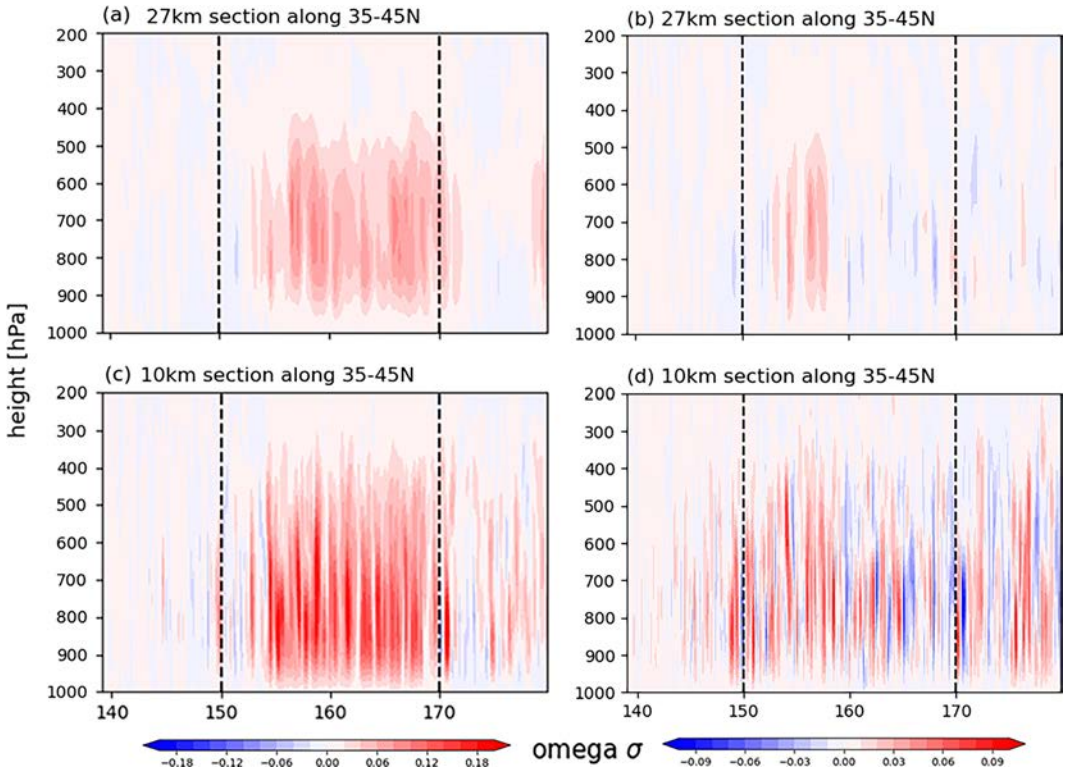

FIG. 10. Meridional average over the SST box of the difference in standard deviation of the vertical velocity (Pa s^{-1}) between the response to the highest and lowest spatially averaged SST at (a) 27- and (c) 10-km resolution, and between the response to corresponding residual SST at (b) 27- and (d) 10-km resolution. The dashed vertical lines indicate the zonal extent of the prescribed SST anomaly. Note the change of scale.

the OE index (OEI) (taken from Hall et al. 2025), albeit positive, is not significant, which reflects that the 20 FDI/SST states considered here were solely chosen on the basis of their high absolute FDI.

There are several caveats in this study. The WRF domain is small, and field evolutions are strongly constrained by the prescribed lateral boundary conditions, which likely limits response amplitude and prevents estimating remote responses. The simulations pertain to February conditions, and different months may lead to different conclusions. Also, they only last 1 month, which may be too short for eddy-mean flow interactions to fully develop and may explain why the response is baroclinic. Last, the SST is only prescribed at 0.25° resolution, after some smoothing (Reynolds et al. 2007), which may be adequate for the model at 27-km resolution but too coarse at 10-km resolution. Hence, possible submesoscale SST impacts may be underestimated in our simulations.

Longer simulations with higher-resolution SSTs and a more extended, if possible global, domain are needed to verify whether oceanic mesoscales near WBCs indeed have little influence on the large-scale atmospheric circulation response to their variability. In addition, only differences between warm and cold SSTs were estimated, and possible

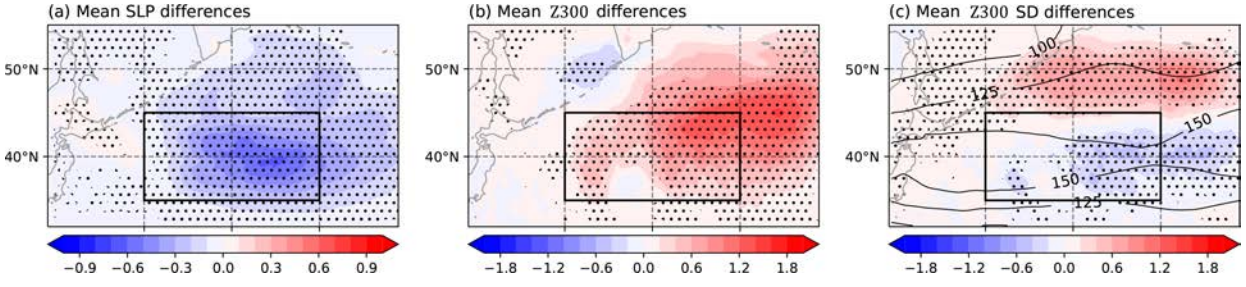

FIG. 11. (a) Mean SLP (hPa), (b) Z300 (m), and (c) standard deviation of Z300 (m) response differences between the SST composites. Contours in (c) denote the averaged standard deviation of Z300 (m). Dots indicate FDR significance at the 5% level, and the rectangle denotes the location of the SST anomalies.

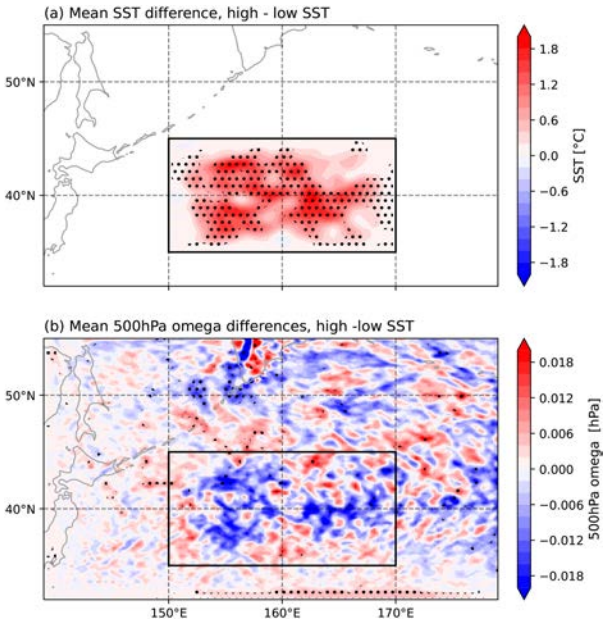

FIG. 12. (top) Mean SST (K) and (bottom) vertical velocity at 500-hPa (Pa s^{-1}) difference between the SST composites. Dots indicate FDR significance at the 5% level, and the rectangle denotes the SST anomaly location.

asymmetries of the response to warm and cold SST should be investigated.

Acknowledgments. This research was funded by the National Science Foundation (NSF) and GEO-NERC through Grant AGS-2040073, and through the U.K. Natural Environment Research Council Grant NE/W004836/1. We thank the editor, Robert Jnglin Wills, and the anonymous reviewers for their useful comments.

Data availability statement. All data used in this work are available online.

REFERENCES

Booth, J. F., L. Thompson, J. Patoux, and K. A. Kelly, 2012: Sensitivity of midlatitude storm intensification to perturbations in the sea surface temperature near the Gulf Stream. *Mon. Wea. Rev.*, **140**, 1241–1256, https://doi.org/10.1175/MWR-D-11-00195.1.

Bui, H., and T. Spengler, 2021: On the influence of sea surface temperature distributions on the development of extratropical cyclones. *J. Atmos. Sci.*, **78**, 1173–1188, https://doi.org/10.1175/JAS-D-20-0137.1.

Chakravorty, S., A. Czaja, R. Parfitt, and W. K. Dewar, 2024: Tropospheric response to Gulf Stream intrinsic variability: A model ensemble approach. *Geophys. Res. Lett.*, **51**, e2023GL107726, https://doi.org/10.1029/2023GL107726.

Chelton, D. B., M. G. Schlax, M. H. Freilich, and R. F. Milliff, 2004: Satellite measurements reveal persistent small-scale features in ocean winds. *Science*, **303**, 978–983, https://doi.org/10.1126/science.1091901.

Chen, S.-H., and W.-Y. Sun, 2002: A one-dimensional time dependent cloud model. *J. Meteor. Soc. Japan*, **80**, 99–118, https://doi.org/10.2151/jmsj.80.99.

Czaja, A., C. Frankignoul, S. Minobe, and B. Vannière, 2019: Simulating the midlatitude atmospheric circulation: What might we gain from high-resolution modeling of air-sea interactions? *Curr. Climate Change Rep.*, **5**, 390–406, https://doi.org/10.1007/s40641-019-00148-5.

Famoos Paolini, L., P. J. Athanasiadis, P. Ruggieri, and A. Bellucci, 2022: The atmospheric response to meridional shifts of the Gulf stream SST front and its dependence on model resolution. *J. Climate*, **35**, 6007–6030, https://doi.org/10.1175/JCLI-D-21-0530.1.

Foussard, A., G. Lapeyre, and R. Plougonven, 2019: Storm track response to oceanic eddies in idealized atmospheric simulations. *J. Climate*, **32**, 445–463, https://doi.org/10.1175/JCLI-D-18-0415.1.

Frankignoul, C., N. Sennéchael, Y.-O. Kwon, and M. A. Alexander, 2011: Influence of the meridional shifts of the Kuroshio and the Oyashio Extensions on the atmospheric circulation. *J. Climate*, **24**, 762–777, https://doi.org/10.1175/2010JCLI3731.1.

Hall, R. J., A. Czaja, G. Danabasoglu, C. Deser, C. Frankignoul, and Y.-O. Kwon, 2025: A new robust frontal disturbance index of the Oyashio Extension sea surface temperature front. *J. Climate*, **38**, 293–307, https://doi.org/10.1175/JCLI-D-23-0642.1.

Haualand, K. F., and T. Spengler, 2020: Direct and indirect effects of surface fluxes on moist baroclinic development in an idealized framework. *J. Atmos. Sci.*, **77**, 3211–3225, https://doi.org/10.1175/JAS-D-19-0328.1.

Hersbach, H., and Coauthors, 2020: The ERA5 global reanalysis. *Quart. J. Roy. Meteor. Soc.*, **146**, 1999–2049, https://doi.org/10.1002/qj.3803.

Hong, S.-Y., Y. Noh, and J. Dudhia, 2006: A new vertical diffusion package with an explicit treatment of entrainment processes. *Mon. Wea. Rev.*, **134**, 2318–2341, https://doi.org/10.1175/MWR3199.1.

Iacono, M. J., J. S. Delamere, E. J. Mlawer, M. W. Shephard, S. A. Clough, and W. D. Collins, 2008: Radiative forcing by long-lived greenhouse gases: Calculations with the AER radiative transfer models. *J. Geophys. Res.*, **113**, D13103, https://doi.org/10.1029/2008JD009944.

Jimenez, P. A., J. Dudhia, J. F. Gonzalez-Rouco, J. Navarro, J. P. Montavez, and E. Garcia-Bustamante, 2012: A revised scheme for the WRF surface layer formulation. *Mon. Wea. Rev.*, **140**, 898–918, https://doi.org/10.1175/MWR-D-11-00056.1.

Joyce, T. M., Y.-O. Kwon, and L. Yu, 2009: On the relationship between synoptic wintertime atmospheric variability and path shifts in the Gulf Stream and the Kuroshio Extension. *J. Climate*, **22**, 3177–3192, https://doi.org/10.1175/2008JCLI2690.1.

——, ——, H. Seo, H. A, and D. C. C. Ummenhofer, 2019: Meridional Gulf Stream shifts can influence wintertime variability in the North Atlantic storm track and Greenland blocking. *Geophys. Res. Lett.*, **46**, 1702–1708, https://doi.org/10.1029/2018GL081087.

Kelly, K. A., R. J. Small, R. M. Samelson, B. Qiu, T. M. Joyce, Y.-O. Kwon, and M. F. Cronin, 2010: Western boundary currents and frontal air–sea interaction: Gulf Stream and Kuroshio Extension. *J. Climate*, **23**, 5644–5667, https://doi.org/10.1175/2010JCLI3346.1.

Kuwano-Yoshida, A., and S. Minobe, 2017: Storm-track response to SST fronts in the northwestern Pacific region in an AGCM. *J. Climate*, **30**, 1081–1102, https://doi.org/10.1175/JCLI-D-16-0331.1.

Kwon, Y.-O., M. A. Alexander, N. A. Bond, C. Frankignoul, H. Nakamura, B. Qiu, and L. A. Thompson, 2010: Role of the Gulf Stream and Kuroshio–Oyashio systems in large-scale atmosphere–ocean interaction: A review. *J. Climate*, **23**, 3249–3281, https://doi.org/10.1175/2010JCLI3343.1.

Larson, J. G., D. W. J. Thompson, and J. W. Hurrell, 2024: Signature of the western boundary currents in local climate variability. *Nature*, **634**, 862–867, https://doi.org/10.1038/s41586-024-08019-2.

Liu, X., and Coauthors, 2021: Ocean fronts and eddies force atmospheric rivers and heavy precipitation in western North America. *Nat. Commun.*, **12**, 1268, https://doi.org/10.1038/s41467-021-21504-w.

Ma, X., and Coauthors, 2015: Distant influence of Kuroshio eddies on North Pacific weather patterns? *Sci. Rep.*, **5**, 17785, https://doi.org/10.1038/srep17785.

——, P. Chang, R. Saravanan, R. Montuoro, H. Nakamura, D. Wu, X. Lin, and L. Wu, 2017: Importance of resolving Kuroshio front and eddy influence in simulating the North Pacific storm track. *J. Climate*, **30**, 1861–1880, https://doi.org/10.1175/JCLI-D-16-0154.1.

O'Reilly, C. H., and A. Czaja, 2015: The response of the Pacific storm track and atmospheric circulation to Kuroshio Extension variability. *Quart. J. Roy. Meteor. Soc.*, **141**, 52–66, https://doi.org/10.1002/qj.2334.

Parfitt, R., A. Czaja, S. Minobe, and A. Kuwano-Yoshida, 2016: The atmospheric frontal response to SST perturbations in the Gulf Stream region. *Geophys. Res. Lett.*, **43**, 2299–2306, https://doi.org/10.1002/2016GL067723.

Piazza, M., L. Terray, J. Boé, E. Maisonnave, and E. Sanchez-Gomez, 2016: Influence of small-scale North Atlantic sea surface temperature patterns on the marine boundary layer and free troposphere: A study using the atmospheric ARPEGE model. *Climate Dyn.*, **46**, 1699–1717, https://doi.org/10.1007/s00382-015-2669-z.

Powers, J. G., and Coauthors, 2017: The Weather Research and Forecasting model: Overview, system efforts, and future directions. *Bull. Amer. Meteor. Soc.*, **98**, 1717–1737, https://doi.org/10.1175/BAMS-D-15-00308.1.

Révelard, A., C. Frankignoul, N. Sennéchael, Y.-O. Kwon, and B. Qiu, 2016: Influence of the decadal variability of the Kuroshio Extension on the atmospheric circulation in the cold season. *J. Climate*, **29**, 2123–2144, https://doi.org/10.1175/JCLI-D-15-0511.1.

Reynolds, R. W., T. M. Smith, C. Liu, D. B. Chelton, K. S. Casey, and M. G. Schlax, 2007: Daily high-resolution-blended analyses for sea surface temperature. *J. Climate*, **20**, 5473–5496, https://doi.org/10.1175/2007JCLI1824.1.

Schemm, S., 2023: Toward eliminating the decades-old "too zonal and too equatorward" storm-track bias in climate models. *J. Adv. Model. Earth Syst.*, **15**, e2022MS003482, https://doi.org/10.1029/2022MS003482.

Seo, H., and Coauthors, 2023: Ocean mesoscale and Frontal-Scale Ocean–Atmosphere Interactions and influence on large-scale climate: A review. *J. Climate*, **36**, 1981–2013, https://doi.org/10.1175/JCLI-D-21-0982.1.

Skamarock, W. C., and Coauthors, 2008: A description of the Advanced Research WRF version 3. NCAR Tech. Note NCAR/TN-475+STR, 113 pp., https://doi.org/10.5065/D68S4MVH.

Small, R. J., and Coauthors, 2008: Air–sea interaction over ocean fronts and eddies. *Dyn. Atmos. Oceans*, **45**, 274–319, https://doi.org/10.1016/j.dynatmoce.2008.01.001.

——, R. A. Tomas, and F. O. Bryan, 2014: Storm track response to ocean fronts in a global high-resolution climate model. *Climate Dyn.*, **43**, 805–828, https://doi.org/10.1007/s00382-013-1980-9.

——, R. Msadek, Y.-O. Kwon, J. F. Booth, and C. Zarzycki, 2019: Atmosphere surface storm track response to resolved ocean mesoscale in two sets of global climate model experiments. *Climate Dyn.*, **52**, 2067–2089, https://doi.org/10.1007/s00382-018-4237-9.

Sroka, S., A. Czaja, and S. Chakravorty, 2022: Assessing the importance of mesoscale sea-surface temperature variations for surface turbulent cooling of the Kuroshio Extension in wintertime. *Quart. J. Roy. Meteor. Soc.*, **148**, 2742–2754, https://doi.org/10.1002/qj.4333.

Taguchi, B., H. Nakamura, M. Nonaka, N. Komori, A. Kuwano-Yoshida, K. Takaya, and A. Goto, 2012: Seasonal evolutions of atmospheric response to decadal SST anomalies in the North Pacific subarctic frontal zone: Observations and a coupled model simulation. *J. Climate*, **25**, 111–139, https://doi.org/10.1175/JCLI-D-11-00046.1.

Tewari, M., and Coauthors, 2004: Implementation and verification of the unified Noah land-surface model in the WRF model. *20th Conf. on Weather Analysis and Forecasting/16th Conf. on Numerical Weather Prediction*, Seattle, WA, Amer. Meteor. Soc., 11–15, https://opensky.ucar.edu/islandora/object/conference%3A1576.

Tsopouridis, L., C. Spensberger, and T. Spengler, 2021: Cyclone intensification in the Kuroshio region and its relation to the sea surface temperature front and upper-level forcing. *Quart. J. Roy. Meteor. Soc.*, **147**, 485–500, https://doi.org/10.1002/qj.3929.

Wilks, D. S., 2016: "The stippling shows statistically significant grid points": How research results are routinely overstated and overinterpreted, and what to do about it. *Bull. Amer. Meteor. Soc.*, **97**, 2263–2273, https://doi.org/10.1175/BAMS-D-15-00267.1.

Willison, J., W. A. Robinson, and G. M. Lackmann, 2013: The importance of resolving mesoscale latent heating in the North Atlantic storm track. *J. Atmos. Sci.*, **70**, 2234–2250, https://doi.org/10.1175/JAS-D-12-0226.1.

Wills, R. C. J., A. R. Herrington, I. R. Simpson, and D. S. Battisti, 2024: Resolving weather fronts increases the large-scale circulation response to Gulf Stream SST anomalies in variable-resolution CESM2 simulations. *J. Adv. Model. Earth Syst.*, **16**, e2023MS004123, https://doi.org/10.1029/2023MS004123.

Wills, S. M., and D. W. J. Thompson, 2018: On the observed relationships between wintertime variability in Kuroshio–Oyashio Extension sea surface temperatures and the atmospheric circulation over the North Pacific. *J. Climate*, **31**, 4669–4681, https://doi.org/10.1175/JCLI-D-17-0343.1.

——, ——, and L. M. Ciasto, 2016: On the observed relationships between variability in Gulf stream sea surface temperatures and the atmospheric circulation over the North Atlantic. *J. Climate*, **29**, 3719–3730, https://doi.org/10.1175/JCLI-D-15-0820.1.

Xie, S., 2004: Satellite observations of cool ocean–atmosphere interaction. *Bull. Amer. Meteor. Soc.*, **85**, 195–208, https://doi.org/10.1175/BAMS-85-2-195.

Zhang, C., and Y. Wang, 2017: Projected future changes of tropical cyclone activity over the western North and South pacific in a 20-km-mesh regional climate model. *J. Climate*, **30**, 5923–5941, https://doi.org/10.1175/JCLI-D-16-0597.1.